FAST, VARIATION-BASED METHODS FOR THE ANALYSIS OF EXTENDED BRAIN SOURCES

Hanna Becker [*,†]*, Laurent Albera* [‡,§,¶]*, Pierre Comon* [†]*, Rémi Gribonval* [¶]*, Isabelle Merlet* [‡,§]

[*] Univ. Nice Sophia Antipolis, CNRS, I3S, UMR 7271, F-06900 Sophia Antipolis, France
[†] GIPSA-Lab, CNRS UMR5216, Grenoble Campus, St Martin d'Heres, F-38402;
[‡] INSERM, U1099, Rennes, F-35000, France;
[§] Université de Rennes 1, LTSI, Rennes, F-35000, France;
[¶] INRIA, Centre Inria Rennes - Bretagne Atlantique, France.

ABSTRACT

Identifying the location and spatial extent of several highly correlated and simultaneously active brain sources from electroencephalographic (EEG) recordings and extracting the corresponding brain signals is a challenging problem. In a recent comparison of source imaging techniques, the VB-SCCD algorithm, which exploits the sparsity of the variational map of the sources, proved to be a promising approach. In this paper, we propose several ways to improve this method. In order to adjust the size of the estimated sources, we add a regularization term that imposes sparsity in the original source domain. Furthermore, we demonstrate the application of ADMM, which permits to efficiently solve the optimization problem. Finally, we also consider the exploitation of the temporal structure of the data by employing $L_{1,2}$-norm regularization. The performance of the resulting algorithm, called $L_{1,2}$-SVB-SCCD, is evaluated based on realistic simulations in comparison to VB-SCCD and several state-of-the-art techniques for extended source localization.

Index Terms— EEG, extended source localization, ADMM, sparsity

1. INTRODUCTION

Over the last decades, a large number of methods have been proposed to reconstruct the electric activity everywhere within the brain based on surface electroencephalographic (EEG) measurements (see e.g. [1] and references therein). This process is generally referred to as source imaging and permits to identify the brain regions which are involved in generating characteristic activity patterns such as epileptic spikes, which is of clinical importance. However, in order to delineate the seizure onset zone in epileptic patients, it is not only important to localize the foci of the epileptogenic sources, but also to identify their spatial extent. This is particularly challenging in the context of several highly correlated, simultaneously active source regions corresponding to epileptic activity that spreads from one region to another.

In a recent comparison of different source imaging algorithms [1], the VB-SCCD algorithm [2] showed a good performance for the localization of extended sources. Moreover, it permits to simultaneously localize several highly correlated active source regions, which is problematic with other extended source localization methods such as STWV-DA [1] and 4-ExSo-MUSIC [3]. Therefore, VB-SCCD is one of the most promising approaches for the identification of multiple active brain regions in the context of propagation phenomena. However, the algorithm shows some difficulties in separating close sources and tends to combine them into one large source. Furthermore, the implementation of VB-SCCD using Second Order Cone Programming (SOCP) [4] as proposed in [2] leads to a high computational complexity, which practically forbids the application of the method for large numbers of time samples.

In this paper, we improve on these points by proposing a new source imaging algorithm, subsequently referred to as sparse VB-SCCD (SVB-SCCD), which includes an additional L_1-norm regularization term. Such an approach, also known as sparse Total Variation (sparse TV) regularization [5], TV-L_1 regularization [6] or fused LASSO [7], has previously been used in image processing [8] and fMRI prediction [5, 6], where it has been shown to lead to robust solutions, but is new in the field of brain source imaging. Note though that the combination of sparsity in the original source domain and in a transformed domain that is different from the total variation has been explored in [9] for MEG source imaging. As shown in this paper, the SVB-SCCD method permits to obtain more focal source estimates than VB-SCCD and achieves the separation of even close sources. Furthermore,

we demonstrate the use of a different optimization technique, called Alternating Direction Method of Multipliers (ADMM) [10], which is much faster than SOCP. This gain on computational complexity enables us to apply the algorithm to large time intervals and to reconstruct the source signals. It also makes it possible to take into account the temporal structure of the data by employing an $L_{1,2}$-norm regularization as first suggested in [11], leading to more robust source estimates. The superior performance of the resulting $L_{1,2}$-SVB-SCCD algorithm in comparison to VB-SCCD, STWV-DA, 4-ExSo-MUSIC, and cLORETA [12] is demonstrated by means of computer simulations, which are conducted in the context of a realistic head model and highly correlated extended sources emitting epileptic spike activity.

2. DATA MODEL AND PROBLEM FORMULATION

The electric potential at the surface of the scalp is characterized by the superposition of signals originating from all over the brain. As most of these signals are generated by pyramidal cells located in the gray matter, for modeling purposes, we define a source space that consists of D dipoles located on the cortical surface with a fixed orientation perpendicular to this surface (see also [13]). More particularly, the dipoles are positioned at the centroids of the triangles of a cortical surface mesh. The EEG measurements $\mathbf{X} \in \mathbb{R}^{N \times T}$ recorded with N sensors for T time samples can then be modeled as a weighted sum of the dipole signals. The weights depend on the propagation effects within the head volume conductor and are summarized in the so-called lead field matrix $\mathbf{G} \in \mathbb{R}^{N \times D}$, which can be computed numerically using boundary element methods (BEM) [14]. Distinguishing two types of cerebral activity, the signals of interest (e.g., epileptic activity) and the background activity of the brain, characterized by the matrices $\mathbf{S} \in \mathbb{R}^{D \times T}$ and $\mathbf{S}_b \in \mathbb{R}^{D \times T}$, respectively, this leads to the following data model:

$$\mathbf{X} = \mathbf{GS} + \mathbf{GS}_b$$
$$= \mathbf{GS} + \mathbf{N}. \tag{1}$$

The objective of source imaging algorithms consists in estimating the signal matrix $\mathbf{S}$ from the measurements $\mathbf{X}$. As the number of dipoles ($D \sim 10000$) is generally much larger than the number of sensors ($N \sim 100$), this is an ill-posed problem, which requires additional assumptions to regularize the solution. In this paper, we consider several approaches based on sparsity, which are described in the next section.

3. SOURCE LOCALIZATION AND EXTRACTION

3.1. VB-SCCD

The VB-SCCD algorithm [2] assumes a piece-wise constant spatial source distribution, which is achieved by imposing sparsity on the variational map of the sources. The latter can

be computed by applying a linear transform, characterized by the matrix $\mathbf{V}$, to the source distribution, which is equivalent to computing the total variation on the discretized cortical surface. The elements $V_{p,d}$ of $\mathbf{V}$, $p = 1, \ldots, P$, $d = 1, \ldots, D$, where P is the number of edges of the triangular grid, are given by:

$$V_{p,d} = \begin{cases} 1 & \text{if } d = d_{p,1} \\ -1 & \text{if } d = d_{p,2} \\ 0 & \text{otherwise} \end{cases} \tag{2}$$

where $d_{p,1}$ and $d_{p,2}$ are the indices of the dipoles sharing the p-th edge. Thus, $\mathbf{VS}$ describes the differences in amplitude between adjacent dipoles. This gives rise to the VB-SCCD cost function, which is minimized with respect to the signal matrix $\mathbf{S}$ [1]:

$$\min_{\mathbf{S}} \frac{1}{2}||\mathbf{X} - \mathbf{GS}||_{\mathrm{F}}^2 + \lambda||\mathbf{VS}||_1. \tag{3}$$

The regularization parameter λ balances between the reconstruction error and the constraint, corresponding to the first and second term in (3), respectively. As suggested in [2], this parameter may be adjusted according to the acceptable upper limit for the reconstruction error, which depends on the noise level.

3.2. SVB-SCCD

In practice, it is reasonable to assume that only a small number of the source dipoles contribute to the signals of interest. Hence, we introduce an additional regularization term in (3) that imposes sparsity in the original source domain, leading to the following optimization problem which is equivalent to the sparse TV [5] or fused LASSO [7] approach:

$$\min_{\mathbf{S}} \frac{1}{2}||\mathbf{X} - \mathbf{GS}||_{\mathrm{F}}^2 + \lambda(||\mathbf{VS}||_1 + \alpha||\mathbf{S}||_1). \tag{4}$$

This approach does not only permit us to adjust the size of the reconstructed source regions by varying the new regularization parameter α, but also prevents the estimated signal vector from being amplitude-biased, which is a problem that frequently arises using the VB-SCCD algorithm. Setting $\alpha = 1$ leads to very focal source estimates, whereas small α only avoid the amplitude bias, but do not influence the size of the reconstructed source regions. In our experience, reasonable results can be achieved for $0.01 \leq \alpha \leq 1$. As for VB-SCCD, the regularization parameter λ regulates the impact of the source priors and is tuned depending on the noise level.

3.3. Exploitation of temporal structure

The VB-SCCD and SVB-SCCD algorithms as described in the previous sections consider each time sample indepen-

---

[1]Please note that we use a different formulation of the optimization problem than employed in [2], but which leads to equivalent results for an appropriate value of the regularization parameter λ. Furthermore, the optimization problem was originally stated for only one time sample.

dently and thus do not take into account the temporal structure of the data. However, it can be expected that in the considered time interval, the active source regions stay the same. This hypothesis can be enforced by replacing the L_1-norm in the above equations by the $L_{1,2}$-norm, which is defined as follows: $||\mathbf{S}||_{1,2} = \sum_{d=1}^{D} \sqrt{\sum_{t=1}^{T} S_{d,t}^2}$. This permits to obtain more robust source estimates. The resulting source localization approach is subsequently called $L_{1,2}$-SVB-SCCD.

3.4. Optimization using ADMM

The optimization problems of the three different algorithms, VB-SCCD, SVB-SCCD, and $L_{1,2}$-SVB-SCCD, can be rewritten in a generalized, constrained optimization framework with latent variables $\mathbf{Y}$ and $\mathbf{Z}$:

$$\min_{\mathbf{S}} \frac{1}{2}||\mathbf{X} - \mathbf{GS}||_{\mathrm{F}}^2 + \lambda(f(\mathbf{Y}) + \alpha f(\mathbf{Z}))$$
$$\text{s. t.} \quad \mathbf{Y} = \mathbf{VS}, \quad \mathbf{Z} = \mathbf{S}. \qquad (5)$$

Here, f represents the regularizing function that is either the L_1 norm (for SVB-SCCD) or the $L_{1,2}$-norm (for $L_{1,2}$-SVB-SCCD). Note that the VB-SCCD optimization problem can be regarded as a special case of (5) where $\alpha = 0$. Problem (5) can be solved using ADMM [10], which is a simple and efficient algorithm for constrained convex optimization. It is based on the idea of alternatingly updating the variables $\mathbf{S} \in \mathbb{R}^{D \times T}$, $\mathbf{Y} \in \mathbb{R}^{P \times T}$, and $\mathbf{Z} \in \mathbb{R}^{D \times T}$ in the augmented Lagrangian of (5), as well as computing alternating updates of the scaled Lagrangian multipliers $\mathbf{U} \in \mathbb{R}^{P \times T}$ and $\mathbf{W} \in \mathbb{R}^{D \times T}$. After initialization (for example, by setting all variables to zero), at the k-th iteration, the following update rules can be derived:

$$\mathbf{S}^{(k+1)} = \mathbf{P}^{-1}\left[\mathbf{G}^\mathrm{T}\mathbf{X} + \rho\mathbf{V}^\mathrm{T}(\mathbf{Y}^{(k)} - \mathbf{U}^{(k)}) + \rho(\mathbf{Z}^{(k)} - \mathbf{W}^{(k)})\right]$$
$$\text{with} \quad \mathbf{P} = \mathbf{G}^\mathrm{T}\mathbf{G} + \rho(\mathbf{V}^\mathrm{T}\mathbf{V} + \mathbf{I})$$
$$\mathbf{Y}^{(k+1)} = \mathrm{prox}_{f,\lambda/\rho}\left(\mathbf{VS}^{(k+1)} + \mathbf{U}^{(k)}\right)$$
$$\mathbf{Z}^{(k+1)} = \mathrm{prox}_{f,\lambda\alpha/\rho}\left(\mathbf{S}^{(k+1)} + \mathbf{W}^{(k)}\right)$$
$$\mathbf{U}^{(k+1)} = \mathbf{U}^{(k)} + \mathbf{VS}^{(k+1)} - \mathbf{Y}^{(k+1)}$$
$$\mathbf{W}^{(k+1)} = \mathbf{W}^{(k)} + \mathbf{S}^{(k+1)} - \mathbf{Z}^{(k+1)}$$

where $\rho > 0$ denotes the penalty parameter introduced in the augmented Lagrangian (see [10]). Please note that in practice, the computation of the inverse of the large matrix $\mathbf{P} \in \mathbb{R}^{D \times D}$ should be avoided, for example, by resorting to inversion lemma and matrix decompositions (such as the QR-decomposition) which can be computed efficiently. The updates of $\mathbf{Y}$ and $\mathbf{Z}$ are formulated using the proximity operator, which is given by:

$$\mathrm{prox}_{f,\beta}(\mathbf{Y}) = \arg\min_{\mathbf{X}} \frac{1}{2}||\mathbf{Y} - \mathbf{X}||_{\mathrm{F}}^2 + \beta f(\mathbf{X}). \qquad (6)$$

Solutions to (6) for f corresponding to the L_1-norm or the $L_{1,2}$-norm of $\mathbf{X}$ can be found in [15]. The algorithm is stopped after convergence or a maximal number of iterations is reached.

4. SIMULATIONS

In this section, we compare the performance of SVB-SCCD, VB-SCCD, $L_{1,2}$-SVB-SCCD, $L_{1,2}$-VB-SCCD, STWV-DA, 4-ExSo-MUSIC, and cLORETA based on computer simulations. To this end, EEG data is generated for $N = 91$ electrodes using a realistic head model with three compartments that represent the brain, the skull, and the scalp. The source space consists of $D = 19626$ dipoles corresponding to the triangles of the cortical surface mesh with orientations perpendicular to the cortical surface. A BEM method [2] is used to compute the lead field matrix. We considered three source regions, in the following referred to as patches, each of which is composed of 100 adjacent dipoles. The first patch was attributed an epileptic spike signal comprising $T = 200$ time samples (at 256 Hz sampling frequency) that was segmented from stereotactic EEG (SEEG) recordings of a patient suffering from epilepsy. We then generated 100 different realizations of this signal, one for each patch dipole, by introducing small variations in amplitude and delay. Assuming that the other patches were activated due to a propagation of the epileptic activity of the first patch, we used the same signals for the dipoles of the second and third patch, but introduced a delay of 4 to 24 ms depending on the distance to the first patch. All source dipoles that do not belong to a patch were attributed Gaussian background activity with an amplitude that was adjusted to the amplitude of the SEEG signals between epileptic spikes, thus leading to realistic Signal to Noise Ratio (SNR) such that $||\mathbf{GS}||_{\mathrm{F}}^2/||\mathbf{N}||_{\mathrm{F}}^2 \approx 1$.

The EEG data were spatially prewhitened before applying the source localization algorithms. For both VB-SCCD and SVB-SCCD, the regularization parameter λ was adjusted such that the reconstruction error lies within a confidence interval of 95 to 99 % of the noise power. In the case of SVB-SCCD, we used a fixed parameter $\alpha = 0.67$ because we found that this leads to reasonable results for the considered scenarios. For VB-SCCD, SVB-SCCD, and cLORETA, which provide one source estimate per time sample, we determined the active patches by thresholding the source estimates at the data sample of maximal power, corresponding to the maximum of the epileptic spike. For each identified source region, comprised of adjacent dipoles, we then computed the average of the time signals of all involved source dipoles in order to obtain one estimated time signal per patch. For 4-ExSo-MUSIC, an estimate of the patch signals was computed as $\hat{\mathbf{S}}_p = \mathbf{H}^+\mathbf{X}$. Here, $\mathbf{H}^+$ denotes the pseudoinverse of the spatial mixing matrix $\mathbf{H} \in \mathbb{R}^{N \times R}$ whose r-th column corresponds to the sum of the lead field vectors associated to the dipoles belonging to the r-th estimated patch. No further processing was necessary in case of STWV-DA, as this algorithm already provides a time signal for each estimated extended source at its output.

The performance of the source localization was assessed

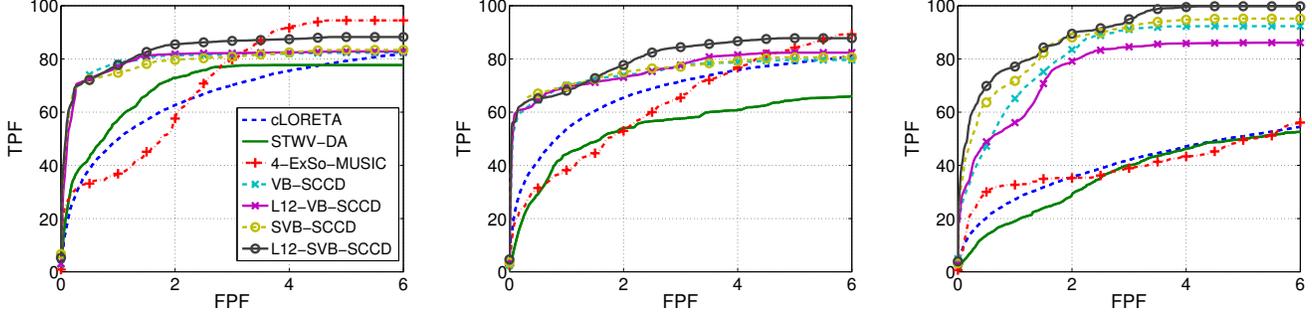
[2]ASA, ANT, Enschede, Netherlands

Fig. 1. ROC curves for (left) scenario 1 (SupFr, InfFr, SupOcc), (middle) scenario 2 (SupOcc, InfPa, InfFr), and (right) scenario 3 (SupOcc, MidTe, OccTe).

using the Dipole Localization Error (DLE) and the Receiver Operating Characteristic (ROC) curves, which evaluate the True Positive Fraction (TPF) as a function of the False Positive Fraction (FPF). If $\mathcal{I}$ and $\hat{\mathcal{I}}$ denote the original and estimated sets of indices of all dipoles belonging to an active patch, $\mathcal{J}$ represents the set of all dipoles belonging to the source space, Q and $\hat{Q}$ are the numbers of original and estimated active dipoles, and $\mathbf{r}_k$ denotes the position of the k-th source dipole, then the DLE, TPF and FPF are defined as:

$$\text{DLE} = \frac{1}{2Q} \sum_{k \in \mathcal{I}} \min_{\ell \in \hat{\mathcal{I}}} ||\mathbf{r}_k - \mathbf{r}_\ell|| + \frac{1}{2\hat{Q}} \sum_{\ell \in \hat{\mathcal{I}}} \min_{k \in \mathcal{I}} ||\mathbf{r}_k - \mathbf{r}_\ell||$$

$$\text{TPF} = \frac{\#(\mathcal{I} \cap \hat{\mathcal{I}})}{\#\mathcal{I}}; \ \text{FPF} = \frac{\#\hat{\mathcal{I}} - \#(\mathcal{I} \cap \hat{\mathcal{I}})}{\#\mathcal{J} - \#\mathcal{I}}.$$

We use the notation $\#\mathcal{I}$ for the cardinality of the set $\mathcal{I}$.

The quality of the extracted signals is evaluated by calculating the correlation coefficients between the estimated patch signal and the averaged signal of all dipoles belonging to a patch. We then computed the mean of the correlation coefficients for all patches.

We simulated three different scenarios with patches of different distances. The first scenario comprised three patches of medium to large distance, located in the superior frontal gyrus (patch SupFr), the inferior frontal gyrus (patch InfFr), and the superior occipital gyrus (SupOcc). The second scenario included two close patches, positioned in the superior occipital and the inferior parietal gyri (patches SupOcc and InfPa), with the third patch in the inferior frontal gyrus (patch InfFr). In the third scenario, we considered three close patches, located in the inferior parietal gyrus (patch InfPa), the mid temporal gyrus (patch MidTe), and the occipital temporal gyrus (patch OccTe). The performance achieved with the different source imaging algorithms in terms of DLE and signal correlation coefficient for the three scenarios, averaged over 30 realizations with different patch signals and background activity, is summarized in Table 1. The corresponding ROC curves are shown in Figure 1. Both the ROC curves and the DLE values show that the VB-SCCD and SVB-SCCD type algorithms clearly outperform the other extended source

	DLE in cm			corr. coeff. in %		
scenario	1	2	3	1	2	3
VB-SCCD	0.99	2.57	9.73	94.9	92.5	78.5
SVB-SCCD	0.94	1.05	3.81	95.5	94.9	89.3
$L_{1,2}$-VB-SCCD	0.97	1.09	10.8	97.9	97.5	77.9
$L_{1,2}$-SVB-SCCD	1.03	1.06	2.24	98.5	98.3	96.6
STWV-DA	10.4	12.3	18.7	65.1	80.1	83.6
4-ExSo-MUSIC	35.3	9.78	9.74	81.0	80.4	74.8
cLORETA	8.69	4.35	13.1	82.5	90.4	45.7

Table 1. Performance of source imaging algorithms in terms of DLE and signal correlation for scenario 1 (SupFr, InfFr, SupOcc), scenario 2 (SupOcc, InfPa, InfFr), and scenario 3 (SupOcc, MidTe, OccTe).

localization approaches for the considered multi-patch scenarios. The use of the additional L_1-norm regularization term in the SVB-SCCD approach turns out to be insignificant in the case of three patches with medium distance (scenario SupFr, InfFr, SupOcc), as SVB-SCCD and VB-SCCD exhibited a comparable performance in this case. However, for two close patches (scenario SupOcc, InfPa, InfFr), one can observe a slight improvement of the DLE obtained with SVB-SCCD compared to VB-SCCD, and for three close patches, the SVB-SCCD approach clearly leads to better results than VB-SCCD. This can also be seen in Figure 2, where we illustrate an example of the source imaging results obtained with the different methods for the scenario with the three close patches InfPa, MidTe, and OccTe. Obviously, the SVB-SCCD approach provides a better separation of the sources than the VB-SCCD approach. Furthermore, Figure 2 visualizes the difficulties encountered with the other extended source localization methods. While the cLORETA solution exhibits high dipole amplitudes at the three patch locations, it does not correctly recover the patches' extents. STWV-DA finds only two patches, one of which is dislocated and deformed compared to the original patch, whereas 4-ExSo-MUSIC identifies only one patch of overestimated extent. The exploitation of the temporal structure of the data in the VB-SCCD and SVB-SCCD algorithms hardly has an impact on the source localization results of scenarios 1 and 2, but
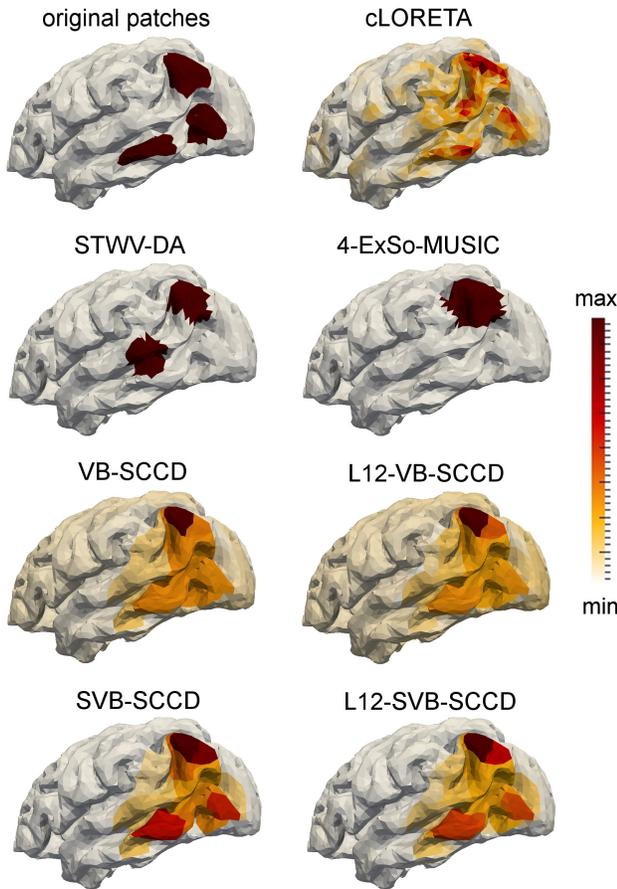
original patches   cLORETA

STWV-DA   4-ExSo-MUSIC

max

min

VB-SCCD   L12-VB-SCCD

SVB-SCCD   L12-SVB-SCCD

Fig. 2. Source imaging results obtained with the different tested algorithms.

for SVB-SCCD, it yields more robust solutions in the case of three close patches (cf. DLE for scenario 3). Furthermore, it leads to a better performance in terms of source extraction as demonstrated by the obtained signal correlation coefficients.

For fixed parameters, the CPU runtimes of the different algorithms are roughly comparable, except for cLORETA, which is faster [3].

5. CONCLUSIONS

In this paper, we have analyzed two extensions of the VB-SCCD algorithm. Following the fused LASSO approach, we have included an additional, sparsity-inducing regularization term, which permits to obtain a better separation of close sources. Furthermore, we have taken into account the temporal structure of the data, which leads to an increased performance in terms of signal extraction. Finally, we have illustrated the use of an efficient algorithm, ADMM, to solve the $L_{1,2}$-SVB-SCCD optimization problem in a much faster way

than the previously employed SOCP algorithm. The superior performance of the proposed approach in comparison to the classic VB-SCCD algorithm as well as other state-of-the-art methods for extended source localization has been demonstrated by means of realistic computer simulations.

REFERENCES

[1] H. Becker, L. Albera, P. Comon, R. Gribonval, F. Wendling, and I. Merlet, "A performance study of various brain source imaging approaches," *IEEE Proc. on ICASSP*, Florence, Italy, May 4-9, 2014.

[2] L. Ding, "Reconstructing cortical current density by exploring sparseness in the transform domain," *Physics in Medicine and Biology*, vol. 54, pp. 2683–2697, 2009.

[3] G. Birot, L. Albera, F. Wendling, and I. Merlet, "Localisation of extended brain sources from EEG/MEG: the ExSo-MUSIC approach," *NeuroImage*, vol. 56, pp. 102–113, 2011.

[4] F. Alizadeh and D. Goldfarb, "Second-order cone programming," Tech. Rep. 51-2001, Rutgers University 2001.

[5] L. Baldassarre, J. Mourao-Miranda, and M. Pontil, "Structured sparsity models for brain decoding from fMRI data," in *IEEE Proc. on PRNI*, London, July 2-4, 2012, pp. 5–8.

[6] A. Gramfort, B. Thirion, and G. Varoquaux, "Identifying predictive regions from fMRI with TV-l_1 prior," in *IEEE Proc. on PRNI*, Philadelphia, June 22-24, 2013, pp. 17–20.

[7] R. Tibshirani and N. Saunders, "Sparsity and smoothness via the fused LASSO," *Journal of the Royal Statistical Society B*, vol. 67, Part I, pp. 91–108, Feb. 2005.

[8] S. Ma, W. Yin, Y. Zhang, and A. Chakraborty, "An efficient algorithm for compressed mr imaging using total variation and wavelets," in *IEEE Proc. on CVPR*, Anchorage, June 23-28, 2008, pp. 1–8.

[9] W. Chang, A. Nummenmaa, J. Hsieh, and F. Lin, "Spatially sparse source cluster modeling by compressive neuromagnetic tomography," *NeuroImage*, vol. 53, no. 1, pp. 146–160, Oct 2010.

[10] S. Boyd, N. Parikh, E. Chu, B. Peleato, and J. Eckstein, "Distributed optimization and statistical learning via alternating direction method of multipliers," *Foundations and Trends in Machine Learning*, vol. 3, no. 1, pp. 1–122, 2010.

[11] E. Ou, M. Hämäläinen, and P. Golland, "A distributed spatio-temporal EEG/MEG inverse solver," *NeuroImage*, vol. 44, 2009.

[12] M. Wagner, M. Fuchs, H. A. Wischmann, and R. Drenck-hahn, "Smooth reconstruction of cortical sources from EEG and MEG recordings," *NeuroImage*, vol. 3, no. 3, pp. S168, 1996.

[13] A. M. Dale and M. I. Sereno, "Improved localization of cortical activity by combining EEG and MEG with MRI cortical surface reconstruction: a linear approach," *Journal of Cognitive Neuroscience*, vol. 5, no. 2, pp. 162–176, 1993.

[14] A. Gramfort, *Mapping, timing and tracking cortical activations with MEG and EEG: Methods and application to human vision*, Ph.D. thesis, Telecom ParisTech, 2009.

[15] A. Gramfort, M. Kowalski, and M. Hämäläinen, "Mixed-norm estimates for the M/EEG inverse problem using accelerated gradient methods," *Physics in Medicine and Biology*, vol. 57, pp. 1937–1961, 2012.

[3]Please note that the CPU times required for the constructions of the Lapacian matrix for cLORETA and of a dictionary of potential sources for STWV-DA and ExSo-MUSIC have not been considered in this analysis.